IEEE Photonics Journal
An IEEE Photonics Society Publication

Open Access

Filtering Property Based on Ultra-Wide Stopband in Double Sector/Sectorial-Ring Stub Resonator Coupled to Plasmonic Waveguide

Volume 9, Number 5, October 2017

Mingfei Zheng
Hongjian Li
Hui Xu
Zhihui He
Zhiquan Chen
Mingzhuo Zhao

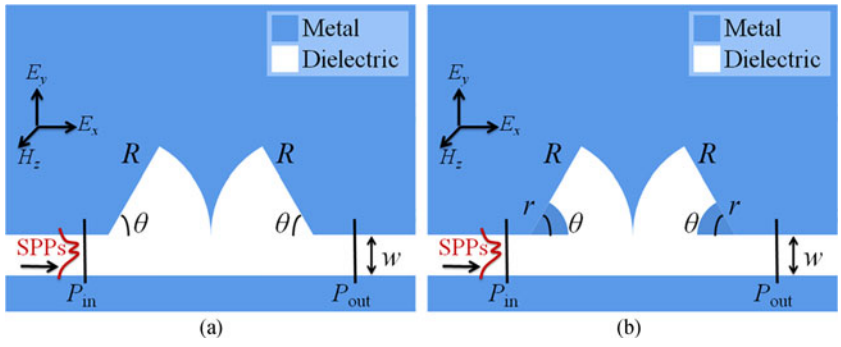

DOI: 10.1109/JPHOT.2017.2739920
1943-0655

Filtering Property Based on Ultra-Wide Stopband in Double Sector/Sectorial-Ring Stub Resonator Coupled to Plasmonic Waveguide

Mingfei Zheng, Hongjian Li, Hui Xu, Zhihui He, Zhiquan Chen, and Mingzhuo Zhao

School of Physics and Electronics, Central South University, Changsha 410083, China

DOI:10.1109/JPHOT.2017.2739920

Manuscript received June 16, 2017; revised August 4, 2017; accepted August 10, 2017. Date of publication August 17, 2017; date of current version October 17, 2017. This work was supported in part by the National Natural Science Foundation of China under Grant 61275174 and in part by the Postgraduate Technology Innovation Project of Central South University under Grant 2017zzts062. Corresponding author: Hongjian Li (e-mail: lihj398@126.com).

Abstract: A double sector or sectorial-ring stub resonator coupled to a plasmonic waveguide is proposed and investigated. This resonator is built with two same stubs that are symmetrically arranged together, which has the advantages of realizing asymmetrical single stub and forming no-distance double stub. The characteristic spectral responses of the two novel systems are simulated by using the finite-difference time-domain method. The results show that an ultra-wide stopband is achieved, and a multiple double stub is realized by altering the structure size of the double stub that plays important role in the stopband phenomenon. A tunable stopband, a specific filtering waveband and an optimum structural parameter are obtained by adjusting the inner radius (r), (outer) radius (R), or central angle (θ) of the double stub. The wavelength and bandwidth of the stopband have various variations with the changing of r, R, or θ, and the stopbands in the two systems have similar changes and different features. This paper provides a promising application for band-stop nanofilters and plasmonic integrated optical circuits.

Index Terms: Plasmonic waveguide, stub resonator, band-stop nanofilter, ultra-wide stopband.

1. Introduction

Surface plasmon polaritons (SPPs), which are a kind of propagating surface electromagnetic waves that are generated and confined at the metal-dielectric interface [1], [2]. Because of SPPs can overcome the diffraction limit in conventional optics and manipulate light at the nanoscale domain [3], [4], which provide possibility to realize nanoscale optical devices with high miniaturization and compact integration in future [5], [6]. In recent years, metal-dielectric-metal (MDM) plasmonic waveguide has attracted people's considerable interest, which can be regarded as a most promising way for realization of nanoscale optical devices and an ideal optical element in integrated optical devices, due to the properties of it that provides a propagation pathway for SPPs, supports an acceptable propagation length for SPPs and confines light at a subwavelength scale [7], [8].

As is well known, the filtering functions of plasmonic nanofilters based on MDM plasmonic waveguide are achieved by the property of wavelength selection [9]–[11]. Different types of plasmonic

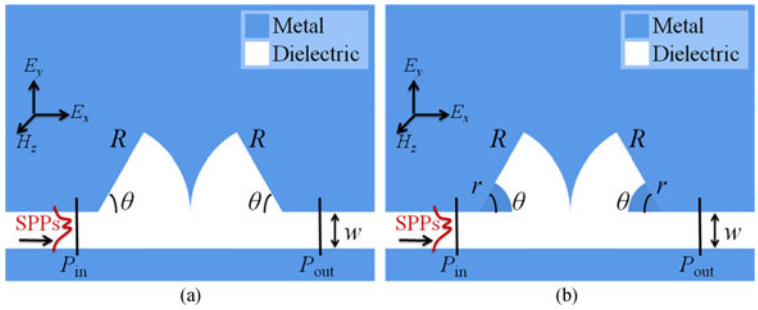

Fig. 1. The 2D schematic of a double (a) SSR or (b) SRSR side-coupled to a MDM plasmonic waveguide.

nanofilters have been discussed theoretically and experimentally, such as band-stop nanofilter [12], band-pass nanofilter [13], low-pass nanofilter [14], and high-pass nanofilter [15]. Recently, a band-stop nanofilter is achieved when MDM plasmonic waveguide coupled with double tooth-shaped [16], symmetrical tooth-shaped [17], periodic teeth-shaped [18], or partitioned rectangle [19] stub resonator. However, these resonators whose complexities are added, stubs are symmetrical shape, distances between each stub are more large, or stopbands are more narrow. Therefore, we first propose a double sector stub resonator (SSR) or sectorial-ring stub resonator (SRSR).

In this letter, we propose a band-stop nanofilter in double SSR or SRSR coupled to MDM plasmonic waveguide, and investigate the characteristic spectral responses of the two novel systems by using the two-dimensional (2D) finite-difference time-domain (FDTD) method with perfectly matched layer (PML) absorbing boundary conditions around all boundaries. An ultra-wide stopband phenomenon is found in the two systems, whose magnetic field distributions are analyzed. Moreover, a tunable stopband is realized in the multiple double stub by changing the geometric parameters of the double stub, whose left-edge wavelength, right-edge wavelength, center wavelength, bandwidth and total tunable bandwidth are analyzed. In addition, the difference and relation between the stopbands in the two systems are discussed. Therefore, the filtering function at different wavebands is realized with a tunable stopband in the band-stop nanofilter, which has potential application in plasmonic integrated optical circuits.

2. Structure Model and Simulation Method

Fig. 1 shows the 2D schematic of the proposed systems, which are composed of a resonator side-coupled to a waveguide. The resonator is a double sector or sectorial-ring stub that is respectively shown in Fig. 1(a) and (b), and the waveguide is a MDM plasmonic waveguide with a straight slot. The double SSR or SRSR is simple and compact structure, which is built with two same stubs that are symmetrically arranged together on the same side of the waveguide. The shape of the single stub is asymmetrical in the x and y directions, which is different from these symmetrical structures of rectangle, square, circle, rectangular-ring, square-ring, circular-ring, and so on. The gap of the double stub is no-distance, which can reduce the structure size of the resonator and shorten the center distance between the two stubs. The main structural parameters are the central angle (θ), (outer) radius (R) and inner radius (r) of the stub, and the width (w) of the waveguide. Two power monitors are respectively set at the inlet and outlet of the waveguide to detect the incident power (P_{in}) and the transmitted power (P_{out}), and the transmittance is defined as $T = P_{out}/P_{in}$. The characteristic spectral responses of the proposed systems are numerically and theoretically investigated by using the FDTD method, and we perform the FDTD simulation with dimension (2D), boundary conditions (PML), time step ($\Delta t = \Delta x/2c$, c is the velocity of light in vacuum), mesh steps ($\Delta x = \Delta y = 5$ nm), source shape (Gaussian) and source injection axis (x-axis).

The blue and white areas of Fig. 1 are metal and dielectric, respectively. The permittivity of metal (ε_m) is approximately described by the Drude model, which is defined as $\varepsilon_m = \varepsilon_\infty - \omega_p{}^2/[\omega(\omega + i\gamma)]$,

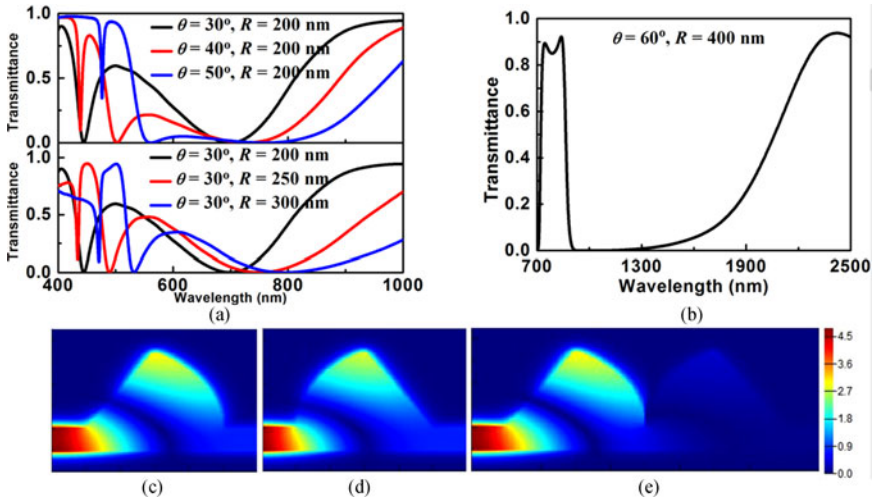

Fig. 2. (a) Transmission spectra of the double SSR system with small size of θ or R. (b) Transmission spectrum of the double SSR system with large size at $\theta = 60^{\circ}$ and $R = 400$ nm. Magnetic field distributions of the (c) left stub, (d) right stub and (e) double stub in the double SSR system with $\theta = 60^{\circ}$ and $R = 400$ nm at $\lambda_C = 1116$ nm.

where ε_∞ is the permittivity of metal at the infinite angular frequency, ω is the angular frequency of incident light, ω_p is the natural frequency of bulk plasma, and γ is the damping frequency of electron collision. The permittivity of dielectric (ε_d) is a constant. To simplify the calculation, the metal and dielectric are assumed to be silver and air, respectively. The parameters for the silver and air can be set as $\varepsilon_\infty = 3.7$, $\omega_p = 1.38 \times 10^{16}$ Hz, $\gamma = 2.73 \times 10^{13}$ Hz and $\varepsilon_d = 1$ that are obtained by fitting experimental results [20], and other parameters for the stub and waveguide are set to be $R \leq 500$ nm and $w = 100$ nm. In addition, the geometric parameters of the left and right stubs in the proposed systems are adjusted simultaneously and identically.

3. Simulation Results and Discussion

To know the transmission spectrum of the double SSR system, we fix the double SSR structure to small size and large size, respectively. The upper and lower of Fig. 2(a) show the transmission spectra of the double SSR system with small size of θ ($\theta = 30^{\circ}$, 40° and 50° when $R = 200$ nm) and R ($R = 200$ nm, 250 nm and 300 nm when $\theta = 30^{\circ}$), respectively. It is found that when $\theta = 30^{\circ}$ and $R = 200$ nm, a very clear transmission peak with a transmission trough occurs at the wavelength range from 450 nm to 700 nm and the transmittance below 0.6. As θ or R increases, the wavelength of the transmission peak shifts toward the long wavelength (red-shift), while the transmittance of the transmission peak continuously decreases. However, the width of the transmission trough continuously increases as θ or R increases. It can be predicted that when the double SSR structure is large size, the transmission peak will completely disappear, while the transmission trough will become more wide that it is seen as a stopband. It will be tried and proven in the next section.

Fig. 2(b) shows the transmission spectrum of the double SSR system with large size at $\theta = 60^{\circ}$ and $R = 400$ nm. It reveals that an ultra-wide stopband phenomenon appears in the novel system of the double SSR structure, and either side of the stopband is a passband whose transmittance is over 0.9. It also proves that the prediction above is correct. The stopband (or bandgap) is defined as the area of wavelengths when the transmittance of transmission spectrum is below 0.01 [21], whose the left-edge wavelength and the right-edge wavelength are labeled as λ_L and λ_R ($\lambda_L < \lambda_R$), respectively. The center wavelength (λ_C) and bandwidth ($\Delta\lambda$) of the stopband are respectively

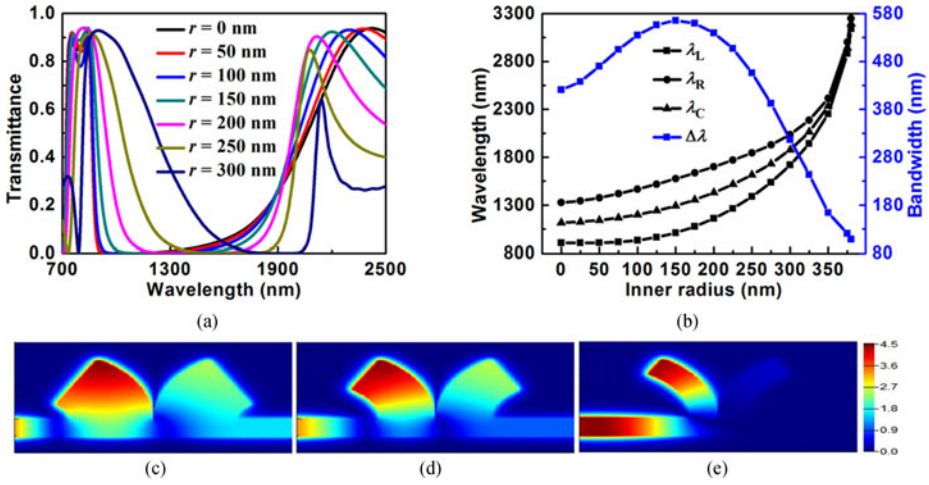

Fig. 3. Transmission characteristics of the double SRSR system with different r when $\theta = 60^{\circ}$ and $R = 400$ nm. (a) Transmission spectra of the stopband. (b) λ_L, λ_R, λ_C and $\Delta\lambda$ of the stopband as functions of r. Magnetic field distributions at $\lambda = 1900$ nm for (c) $r = 100$ nm, (d) $r = 200$ nm and (e) $r = 300$ nm.

defined to be

$$\lambda_C = \frac{1}{2}(\lambda_L + \lambda_R) \tag{1}$$

$$\Delta\lambda = \lambda_R - \lambda_L \tag{2}$$

Therefore, the ultra-wide stopband of the double SSR system occurs at the wavelength range from 906 nm to 1327 nm and around the center wavelength $\lambda_C = 1116$ nm with a bandwidth $\Delta\lambda = 421$ nm.

This ultra-wide stopband implies that a part of SPPs cannot transmit in the proposed double SSR structure. The magnetic field distributions of the left stub, right stub and double stub in the double SSR system with $\theta = 60^{\circ}$ and $R = 400$ nm at $\lambda_C = 1116$ nm are shown in Fig. 2(c)–(e), respectively. When the stub is a single stub (left or right stub), most of the power is confined in the single stub and reflected back to the left of the waveguide, and a few of the power is transported out. When the stub is a double stub, almost all of the power is confined in the left stub and reflected back to the left of the waveguide, and no power is transported out. Moreover, the magnetic field distributions are no difference between the left stub and the right stub, and the magnetic field distribution of the double stub almost is the same as the single left or right stub. That is to say, the magnetic field distribution of the double stub is consistent with the transmission spectrum, and a transmission trough appears in the transmission spectrum of the single left or right stub that just locates at the stopband of the double stub. Therefore, the ultra-wide stopband of the double stub is related to the interaction between the left stub and the right stub, which arises from the destructive interference superposition of the reflected and transmitted waves from each stub. In this case, the proposed double SSR structure can realize a band-stop nanofilter with a typical filtering function, owing to the ultra-wide stopband.

As an extension of the double SSR structure, the double SRSR structure is also proposed whose different part is the inner radius of the stub. To optimize the structure size, the transmission characteristics of the double SRSR system with different inner radii (r) are analyzed. Fig. 3(a) shows the transmission spectra of the stopband in the double SRSR system with different values of r when $\theta = 60^{\circ}$ and $R = 400$ nm. It is found that the stopband is sensitive to the inner radius when r is varied and happens a red-shift as r increases. To explain this phenomenon, we analyze the resonance wavelength (λ_m) of the stub resonator. Using the coupled mode theory (CMT) [22], a single stub can be seen as a Fabry-Perot (FP) resonator, and $\Delta\varphi$ is defined as the total phase delay

per round-trip of SPPs in a single stub resonator, which is described as $\Delta\varphi = 4\pi n_{\text{eff}} l_{\text{eff}}/\lambda_m + \varphi$, where n_{eff} is the effective refractive index of light in the stub or waveguide, l_{eff} is the effective length of SPPs in the stub, and φ is the phase shift of reflected SPPs at the end of the stub. If the stub resonator satisfies the resonance condition as $\Delta\varphi = (2m+1)\cdot\pi$, λ_m at the transmission trough of transmission spectrum is expressed as

$$\lambda_m = \frac{4 n_{\text{eff}} l_{\text{eff}}}{(2m+1) - \varphi/\pi} \tag{3}$$

where m is the order of resonance mode ($m = 0, 1, 2 \ldots$). In view of λ_m is closely related to n_{eff} and l_{eff}, we need to discuss n_{eff} and l_{eff}. n_{eff} can be obtained by the dispersion relation, which is defined as (take real part to calculate) [23]

$$\varepsilon_{\text{m}}\sqrt{n_{\text{eff}}{}^2 - \varepsilon_{\text{d}}}\,\tanh\left(\frac{w\pi\sqrt{n_{\text{eff}}{}^2 - \varepsilon_{\text{d}}}}{\lambda}\right) + \varepsilon_{\text{d}}\sqrt{n_{\text{eff}}{}^2 - \varepsilon_{\text{m}}} = 0 \tag{4}$$

where w is the width of the stub or waveguide, λ is the wavelength of incident light, ε_{m} and ε_{d} are the permittivities of metal and dielectric, respectively. When w becomes smaller (or larger), n_{eff} becomes larger (or smaller) [24]. l_{eff} can be calculated by the arc length formula, and the center arc lengths of the single stub in the double SSR and double SRSR stand for l_{eff} of the single stub in the two resonators, which are respectively described to be

$$l_{\text{eff1}} = \frac{\theta\pi R}{360^{\text{o}}} \tag{5}$$

$$l_{\text{eff2}} = \frac{\theta\pi\,(R + r)}{360^{\text{o}}} \tag{6}$$

According to (3), (4), and (6), λ_m increases by the increasing of n_{eff} and l_{eff2} as r increases. Therefore, the ultra-wide stopband happens a red-shift, due to λ_m increases as r increases.

To get more transmission characteristics, we analyze the wavelength and bandwidth of the stopband. Fig. 3(b) shows λ_{L}, λ_{R}, λ_{C} and $\Delta\lambda$ of the stopband in the double SRSR system as functions of r (0 nm $\leq r \leq$ 380 nm). Obviously, λ_{L}, λ_{R} and λ_{C} have a same change trend and present a nonlinearly increase as r increases, which are due to the increment of λ_m. According to λ_{C} is close to λ_m [21], the increasing rate (k) of λ_{C} is defined to be

$$k = \frac{\Delta\lambda_{\text{C}}}{\Delta x} \approx \frac{4\left[(\Delta n_{\text{eff}}/\Delta x)\cdot l_{\text{eff}} + n_{\text{eff}}\cdot(\Delta l_{\text{eff}}/\Delta x)\right]}{(2m+1) - \varphi/\pi} \tag{7}$$

where x is the geometric parameter of the double stub. It can be seen from Fig. 3(b) that k increases as r increases, due to the increment of $\Delta n_{\text{eff}}/\Delta r$ and the unchanged $\Delta l_{\text{eff2}}/\Delta r$ that is in line with (7). According to the CMT, the left and right stubs of the double stub can be assumed as two identical FP resonators, which mainly produce the direct coupling of FP resonance between each other when the center distance between the two stubs is small [21], and the bandwidth of the stopband is associated with the strength of the direct coupling of FP resonance between the two stubs. It can be seen from Fig. 3(b) that $\Delta\lambda$ increases first from 421 nm to 566 nm and then decreases from 566 nm to 109 nm as r increases, which is attributed to the direct coupling is enhanced first that results from the coupling lengths of the two stubs increase and the coupling distance between the two stubs decreases, and then weakened that results from the widths of the two stubs decrease. Moreover, the total tunable bandwidth ($\Delta\lambda_{\text{total}}$) of the stopband is defined to be [21]

$$\Delta\lambda_{\text{total}} = \lambda_{\text{R}}\left|_{x_{\text{right}}} - \lambda_{\text{L}}\right|_{x_{\text{left}}} \tag{8}$$

where x_{right} and x_{left} correspond to the maximum value of λ_{R} and the minimum value of λ_{L}, respectively. And $\Delta\lambda_{\text{total}} = \lambda_{\text{R}}|_{r=380\text{nm}} - \lambda_{\text{L}}|_{r=0\text{nm}} = 2342$ nm when λ_{L} or λ_{R} shifts from 906 nm to 3248 nm as r increases. In addition, $\Delta\lambda$ of the double SRSR system can reach the maximum value 566 nm when $r = 150$ nm, which is larger and smaller than the double SSR system when

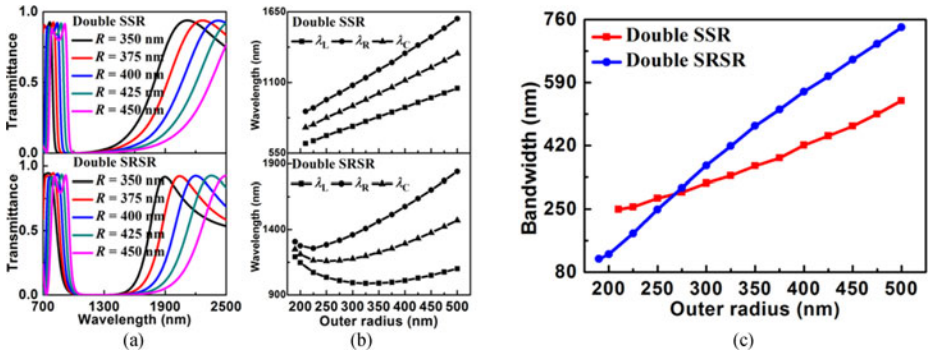

Fig. 4. Transmission characteristics of the double SSR system and double SRSR system with different R when $\theta = 60^{\circ}$ and $r = 150$ nm. (a) Transmission spectra of the stopbands. (b) λ_L, λ_R and λ_C of the stopbands as functions of R. (c) $\Delta\lambda$ of the stopbands as functions of R.

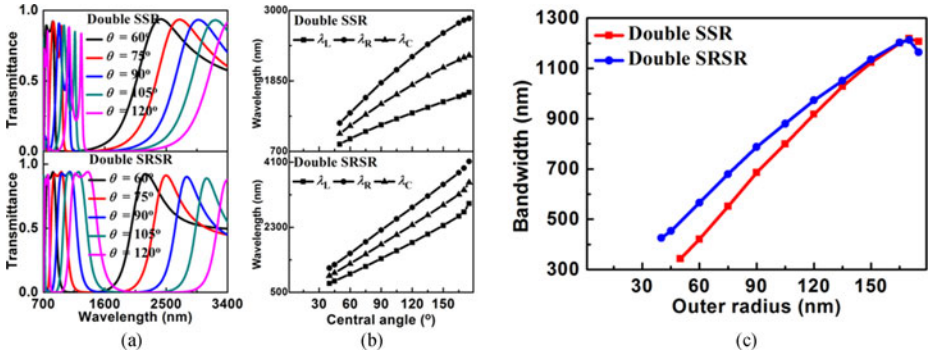

Fig. 5. Transmission characteristics of the double SSR system and double SRSR system with different θ when $R = 400$ nm and $r = 150$ nm. (a) Transmission spectra of the stopbands. (b) λ_L, λ_R and λ_C of the stopbands as functions of θ. (c) $\Delta\lambda$ of the stopbands as functions of θ.

0 nm $< r \leq$ 250 nm and 250 nm $< r \leq$ 380 nm, respectively. And the stopband of the double SRSR system becomes a transmission trough when 380 nm $< r <$ 400 nm. Taking the above factors into consideration, the $r = 150$ nm is an optimum value in the double SRSR system.

Based on the result above, we further study the change process of magnetic field distribution. Fig. 3(c)–(e) show the magnetic field distributions in the double SRSR system at $\lambda = 1900$ nm for r of 100 nm, 200 nm and 300 nm, respectively. When $r = 100$ nm, the transmission spectrum is the passband waveband, all of the power is confined in the double stub and the waveguide, which can be freely transmitted from left to right in the waveguide. As r increases to 200 nm, the transmission is weakened, most of the power is confined in the left stub and reflected back to the left of the waveguide, small part of the power is confined in the right stub and the right of the waveguide, and a few of the power is transported out. As r increases to 300 nm, the transmission is more weakened, almost all of the power is confined in the left stub and reflected back to the left of the waveguide, and no power is transported to the right of the waveguide. Therefore, a tunable stopband, a specific filtering waveband and an optimum structural parameter of the band-stop nanofilter are obtained.

In order to investigate how the structure size of the double stub influences the ultra-wide stopband, we analyze the transmission characteristics of the two systems with various geometric parameters of the double stub, such as the (outer) radius and the central angle. A multiple double stub is realized by altering the structure size of the double stub, which is easy fabrication and convenient adjustment, and plays important role in the stopband phenomenon. For the sake of comparison, we investigate the two systems at the same time. The transmission characteristics of the two systems with different (outer) radii (R) when $\theta = 60^{\circ}$ and $r = 150$ nm, and different central angles (θ) when $R = 400$ nm and $r = 150$ nm are shown in Figs. 4 and 5, respectively.

The transmission spectra of the stopbands in the double SSR system and double SRSR system with different values of R when $\theta = 60^{\circ}$ and $r = 150$ nm are shown in the upper and lower of Fig. 4(a), respectively. Obviously, the stopbands of the two systems happen a red-shift as R increases, which are due to λ_m increases by the increasing of l_{eff} as R increases, although n_{eff} decreases as R increases, and it is in accordance with (3), (4), (5), and (6). λ_{L}, λ_{R} and λ_{C} of the stopbands in the two systems as functions of R ($R \leq 500$ nm) are shown in Fig. 4(b). It can be seen that λ_{L}, λ_{R} and λ_{C} of the two systems have a same change trend and tend to linearly increase as R increases, which are due to the increment of λ_m. It also can be seen that k of the two systems almost unchanges as R increases, due to the unchanged $\Delta n_{\text{eff}}/\Delta R$ and $\Delta l_{\text{eff}}/\Delta R$ that is in accordance with (7), and k of the double SSR system is larger than the double SRSR system. However, λ_{L}, λ_{R}, λ_{C} and k of the double SRSR system with small size of R decrease first and then increase as R increases. $\Delta\lambda$ of the stopbands in the two systems as functions of R are shown in Fig. 4(c). It is found that $\Delta\lambda$ of the two systems almost linearly increase as R increases, which are due to the direct coupling is enhanced that results from the coupling lengths and widths of the two stubs increase. Moreover, as R increases, λ_{L} or λ_{R} of the double SSR system and double SRSR system respectively shift from 625 nm to 1596 nm and from 989 nm to 1840 nm, $\Delta\lambda$ respectively increase from 255 nm to 541 nm and from 116 nm to 739 nm, and $\Delta\lambda_{\text{total}}$ respectively are $\Delta\lambda_{\text{total}} = \lambda_{\text{R}}|_{R=500\text{ nm}} - \lambda_{\text{L}}|_{R=210\text{ nm}} = 971$ nm and $\Delta\lambda_{\text{total}} = \lambda_{\text{R}}|_{R=500\text{ nm}} - \lambda_{L}|_{R=325\text{ nm}} = 851$ nm. In addition, $\Delta\lambda$ can reach maximum value when $R = 500$ nm, and $\Delta\lambda$ of the double SSR system is larger and smaller than the double SRSR system when 210 nm $\leq R \leq$ 275 nm and 275 nm $< R \leq$ 500 nm, respectively. And the stopbands of the double SSR system and double SRSR system don't appear when $R <$ 210 nm and $R <$ 190 nm, respectively. Therefore, the greater R is an optimum value in the two systems.

The upper and lower of Fig. 5(a) respectively show the transmission spectra of the stopbands in the double SSR system and double SRSR system with different values of θ when $R = 400$ nm and $r = 150$ nm. It can be seen that the stopbands of the two systems happen a red-shift as θ increases, which are attributed to λ_m increases by the unchanged n_{eff} and the increasing of l_{eff} as θ increases, and it is in line with (3), (4), (5), and (6). Fig. 5(b) shows λ_{L}, λ_{R} and λ_{C} of the stopbands in the two systems as functions of θ ($\theta \leq 175^{\circ}$). It is found that λ_{L}, λ_{R} and λ_{C} of the two systems have a same change trend and tend to linearly increase as θ increases, which are attributed to the increment of λ_m. It is also found that k of the two systems almost unchanges as θ increases, due to the unchanged $\Delta n_{\text{eff}}/\Delta\theta$ and $\Delta l_{\text{eff}}/\Delta\theta$ that is in line with (7), and k of the double SSR system is smaller than the double SRSR system. Fig. 5(c) shows $\Delta\lambda$ of the stopbands in the two systems as functions of θ. Obviously, $\Delta\lambda$ of the two systems almost linearly increases as θ increases, which are attributed to the direct coupling is enhanced that results from the coupling lengths of the two stubs increase. However, $\Delta\lambda$ decreases when $\theta > 170^{\circ}$ that results from the changed side of the stub is more and more close to the waveguide. Moreover, as θ increases, λ_{L} or λ_{R} of the double SSR system and double SRSR system respectively shift from 818 nm to 2869 nm and from 748 nm to 4122 nm, $\Delta\lambda$ respectively increase from 421 nm to 1218 nm and from 453 nm to 1213 nm, and $\Delta\lambda_{\text{total}}$ respectively are $\Delta\lambda_{\text{total}} = \lambda_{\text{R}}|_{\theta=175^{o}} - \lambda_{\text{L}}|_{\theta=50^{o}} = 2051$ nm and $\Delta\lambda_{\text{total}} = \lambda_{\text{R}}|_{\theta=175^{o}} - \lambda_{\text{L}}|_{\theta=40^{o}} = 3374$ nm. In addition, $\Delta\lambda$ can reach maximum value when $\theta = 170^{\circ}$, and $\Delta\lambda$ of the double SSR system is smaller and larger than the double SRSR system when $50^{\circ} \leq \theta < 170^{\circ}$ and $170^{\circ} \leq \theta \leq 175^{\circ}$, respectively. And the stopbands of the double SSR system and double SRSR system don't appear (or disappear) when $\theta < 50^{\circ}$ and $\theta < 40^{\circ}$, respectively (or when $175^{\circ} < \theta \leq 180^{\circ}$). Therefore, the $\theta = 170^{\circ}$ is an optimum value in the two systems.

4. Conclusion

In conclusion, a band-stop nanofilter in double SSR or SRSR coupled to MDM plasmonic waveguide is proposed. We investigate the characteristic spectral responses of the two novel systems, and find an ultra-wide stopband phenomenon by building a double stub with two same stubs that are symmetrically arranged together. The stopband can be tuned by adjusting the inner radius (r), (outer) radius (R) or central angle (θ) of the double stub, whose wavelength and

bandwidth have various variations with the changing of r, R or θ. For the double SRSR system, as r increases with $\theta = 60^{\circ}$ and $R = 400$ nm, the bandwidth reaches a maximum value of 566 nm when $r = 150$ nm. For the double SSR system and double SRSR system, as R increases ($R \leq 500$ nm) with $\theta = 60^{\circ}$ and $r = 150$ nm, the bandwidths respectively reach the maximum values of 541 nm and 739 nm when $R = 500$ nm; as θ increases with $R = 400$ nm and $r = 150$ nm, the bandwidths respectively reach the maximum values of 1218 nm and 1213 nm when $\theta = 170^{\circ}$. The stopbands in the two systems with the same parameter and variation adjustment have similar changes and different features, and a specific filtering waveband and an optimum structural parameter are obtained. The proposed structures realize asymmetrical single stub, form no-distance double stub and achieve ultra-wide stopband, whose the filtering function at different wavebands is realized. Our results provide a guideline to realize the filtering function by tuning stopband in band-stop nanofilters, and have potential applications in plasmonic integrated optical circuits.

References

[1] W. L. Barnes, A. Dereux, and T. W. Ebbesen, "Surface plasmon subwavelength optics," *Nature*, vol. 424, no. 6950, pp. 824–830, Aug. 2003.

[2] W. L. Barnes, W. A. Murray, J. Dintinger, E. Devaux, and T. W. Ebbesen, "Surface plasmon polaritons and their role in the enhanced transmission of light through periodic arrays of subwavelength holes in a metal film," *Phys. Rev. Lett.*, vol. 92, no. 10, Mar. 2004, Art. no.107401.

[3] J. Park, K. Kim, I. Lee, H. Na, S. Lee, and B. Lee, "Trapping light in plasmonic waveguides," *Opt. Exp.*, vol. 18, no. 2, pp. 598–623, Jan. 2010.

[4] C. Genet and T. W. Ebbesen, "Light in tiny holes," *Nature*, vol. 445, no. 7123, pp. 39–46, Jan. 2007.

[5] J. A. Dionne, L. A. Sweatlock, and H. A. Atwater, "Plasmon slot waveguides: Towards chip-scale propagation with subwavelength–scale localization," *Phys. Rev. B*, vol. 73, no. 3, Jan. 2006, Art. no. 035407.

[6] S. I. Bozhevolnyi, V. S. Volkov, E. Devaux, J. Y. Laluet, and T. W. Ebbesen, "Channel plasmon subwavelength waveguide components including interferometers and ring resonators," *Nature*, vol. 440, no. 7083, pp. 508–511, Mar. 2006.

[7] C. Min and G. Veronis, "Absorption switches in metal-dielectric-metal plasmonic waveguides," *Opt. Exp.*, vol. 17, no. 13, pp. 10757–10766, Jun. 2009.

[8] L. Yang, C. Min, and G. Veronis, "Guided subwavelength slow-light mode supported by a plasmonic waveguide system," *Opt. Lett.*, vol. 35, no. 24, pp. 4184–4186, Dec. 2010.

[9] Z. He *et al.*, "Aspect ratio control and sensing applications for a slot waveguide with a multimode stub," *Appl. Phys. Exp.*, vol. 9, no. 7, Jun. 2016, Art. no. 072002.

[10] Z. Chen *et al.*, "Tunable high quality factor in two multimode plasmonic stubs waveguide," *Sci. Rep.*, vol. 6, Apr. 2016, Art. no. 24446.

[11] H. Xu, H. Li, B. Li, Z. He, Z. Chen, and M. Zheng, "Influential and theoretical analysis of nano-defect in the stub resonator," *Sci. Rep.*, vol. 6, Aug. 2016, Art. no. 30877.

[12] V. F. Nezhad, S. Abaslou, and M. S. Abrishamian, "Plasmonic band-stop filter with asymmetric rectangular ring for WDM networks," *J .Opt.*, vol. 15, no. 5, May 2013, Art. no. 055007.

[13] W. Wang, L. Zhang, L. Shang, and Y. Zhang, "Experimental study of the band-pass filter and slow-wave effect in a MDM channel based on a magnetic plasmonic analogue of EIT," *J. Korean Phys. Soc.*, vol. 67, no. 9, pp. 1544–1552, Nov. 2015.

[14] A. Hosseini, H. Nejati, and Y. Massoud, "Design of a maximally flat optical low pass filter using plasmonic nanostrip waveguides," *Opt. Exp.*, vol. 15, no. 23, pp. 15280–15286, Nov. 2007.

[15] J. Zhu, Q. Wang, P. Shum, and X. Huang, "A nanoplasmonic high-pass wavelength filter based on a metal-insulator-metal circuitous waveguide," *IEEE Trans. Nanotechnol.*, vol. 10, no. 6, pp. 1357–1361, Nov. 2011.

[16] X. Zhai *et al.*, "Tuning bandgap of a double-tooth-shaped MIM waveguide filter by control widths of the teeth," *J. Opt.*, vol. 15, no. 5, Apr. 2013, Art. no. 055008.

[17] L. Cui, G. Song, L. Yu, P. Lang, and J. Xiao, "Tunable band-stop plasmonic filter based on symmetrical tooth-shaped waveguide couples," *Mod. Phys. Lett. B*, vol. 27, no. 14, May 2013, Art. no. 1350101.

[18] H. Wang *et al.*, "Tunable band-stop plasmonic waveguide filter with symmetrical multiple-teeth-shaped structure," *Opt. Lett.*, vol. 41, no. 6, pp. 1233–1236, Mar. 2016.

[19] Z. Chen *et al.*, "Tunable ultra-wide band-stop filter based on single-stub plasmonic-waveguide system," *Appl. Phys. Exp.*, vol. 9, no. 10, Sep. 2016, Art. no. 102002.

[20] E. D. Palik, *Handbook of Optical Constants of Solids*, Boston, MA, USA: Academic, 1985.

[21] M. Zheng, H. Li, Z. Chen, Z. He, H. Xu, and M. Zhao, "Compact and multiple plasmonic nanofilter based on ultra-broad stopband in partitioned semicircle or semiring stub waveguide," *Opt. Commun.*, vol. 402, pp. 47–51, Nov. 2017.

[22] H. A. Haus and W. Huang, "Coupled-mode theory," *Proc. IEEE*, vol. 79, no. 10, pp. 1505–1518, Oct. 1991.

[23] H. Lu, X. Liu, Y. Gong, D. Mao, and L. Wang, "Enhancement of transmission efficiency of nanoplasmonic wavelength demultiplexer based on channel drop filters and reflection nanocavities," *Opt. Exp.*, vol. 19, no. 14, pp. 12885–12890, Jul. 2011.

[24] B. Li *et al.*, "High-sensitivity sensing based on plasmon-induced transparency," *IEEE Photon. J.*, vol. 7, no. 5, Oct. 2015, Art. no. 4801207.